A Calibration Method for Misaligned Scanner Geometry in Cone-beam Computed Tomography

Yi Sun , Ying Hou , Fengyong Zhao , Jiasheng Hu

***Abstract*—Computed Tomography (CT) images often suffer from artifacts caused by misaligned scanner geometry of CT system. Calibration and correction must be done before image reconstruction. A method for calibration of misaligned scanner geometry in cone-beam CT with single-circle orbit is proposed. In this method, a four-point phantom is used to estimate a set of parameters that describe the geometry of a cone-beam CT system. It requires only one projection of the phantom, instead of several projections at multi-angles. An analytical formula is derived, which avoids falling into local minimum. In addition, there is no restriction on any one of the geometric parameters. The simulated results are illustrated. It is proved that this method is applicable and efficient for misaligned scanner.**

***Index Terms*—geometric misalignment, calibration, cone-beam CT**

I. INTRODUCTION

CT technology has made a revolutionary impact on medical diagnosis and also has been successfully used in industrial non-destructive testing. However, CT images often suffer from artifacts. In x-ray CT, it is generally considered that physical effects (beam hardening, scattering, etc.) and instrumentation effects (misalignment and noise, etc.) will cause artifacts [1]. Among these factors, instrumentation misalignment is a major and ubiquitous factor that may lead to artifacts. In cone-beam CT system, it takes special care to ensure that the x-ray focal spot, the center of rotation of the system and the center of the detector fall in a straight line. In practice, however, it is impossible to accurately avoid any misalignment in the CT system. Even a small error in the estimation of any parameter can cause visibly detrimental effects on the reconstructed image. The errors of the displacement and of the rotation of the scanner are so small that it would be very hard to align the scanner geometry accurately with instruments. It is therefore necessary to use mathematical processing of the measured data to simulate the translation and the rotation of the scanner required for proper alignment of the system. This can be achieved simply by applying a rotation translation transformation to each measured radiograph.

To solve this problem, several methods for geometrical calibration of tomographic systems have already been proposed to calculate or estimate the geometry of x-ray CT. Gullberg *et al*.[2] proposed an approach by fitting the calculated projections of a point source to the measured ones by a least squares minimization. In this method, an ideal geometry of camera was assumed except for an electrical shift. Li *et al*. [3] extended Gullberg's method to include the mechanical offset in 1993. Rizo *et al*. [4] gave another method, which can avoid the correlations in the simultaneous estimation of all parameters. A method that measured two 180-deg-opposed cone-beam radiographs of a specially manufactured calibration aperture was proposed by Bronnikov [5]. The method could easily restore its idealized image by applying a certain threshold to the measured data. It also enabled virtual system alignment by using mathematical processing of the measured data, rather than moving the parts of the system. Beque [6] used the projection locations of tomographic acquisition of three point sources located at known distances from each other to estimate the geometry. Marek [7] used matrix notation with homogeneous coordinates to describe the scanner geometry, its misalignment, and the acquisition process. Frederic [8] proposed a method which required a small set of measurements of a simple calibration object consisting of two spherical objects. All of these methods can calibrate or correct misalignments more or less. We can boil down these methods to three characteristics, including assuming a few conditions to be ideal or negligible, solving a set of equations containing six parameters and requiring projections at multi-angles.

In this paper, we propose a new method to estimate all parameters for calibration with a four-point phantom, which can provide necessary and sufficient information for the proposed calibration method. This method requires a projection at only one angle, which avoids the error caused by rotation, to estimate all the parameters of the scanner geometry without solving a set of equations. Most of the time, solving a set of equations may result in local minimum. Thus the calibration procedure is more simple.

The following paper is divided into several parts. In section II we first present the artifacts caused by different kinds of misaligned scanner geometry. Then we describe the cone-beam scanner geometry in section III, including ideal geometry, misaligned geometry and their relationships. Section IV describes principles of our method in detail. In section V, we describe the procedure of calibration and give the simulated results. Finally, this method is further discussed and the conclusion is presented in section VI.

II. ARTIFACTS CAUSED BY MISALIGNMENT

In the ideal geometry of a cone-beam CT system, an x-ray source, rotation center of the system, and center of the detector should fall in a straight line. And the central ray should be perpendicular to the detector surface at the center of the detector.

If there are misalignments in the system, CT images will suffer from artifacts. Different artifacts are caused by different misalignments. We simulate these misalignments and reconstruct the CT images in such conditions. Simulations are done under the following typical scanner geometry: (1) A two-dimensional detector with 576×768 elements of $(0.1458\text{mm})^2$ size each. (2) The distance from the x-ray source to the axis of rotation is 600mm. (3) The distance from the x-ray source

to the detector is 1000mm. (4) 100 slices are recovered with a 0.156mm interval. The 50^{th} slice is the central plane. The images reconstructed by FDK [9] are shown in Fig.1 and Fig.2.

As shown in Fig.1, there are artifacts in distorted image when the detector shifts in the horizontal transverse direction. In image (d), the shape of the artifact is similar to an arc reconstructed incorrectly from a dot. Similar to image (d), reconstructed images in (e) and (f) are distorted. If we divide the circle and square into lots of small points like that in image (d), the artifacts shown in image (e) and (f) could be considered as being composed of artifacts of those small points. That's why the artifacts in (e) and (f) look like a "white area".

In Fig. 2, (a) is the original image of each slice, and (b) is the reconstructed image of the central slice under the ideal scanner geometry. When the detector plane tilts around the central row, the projection of different slices may have the same position on the detector. Using these projection data to reconstruct CT images will reduce the reconstruction precision. Since the central slice is not affected in this situation, we take the 65^{th} slice for example in Fig. 2 (c). When the

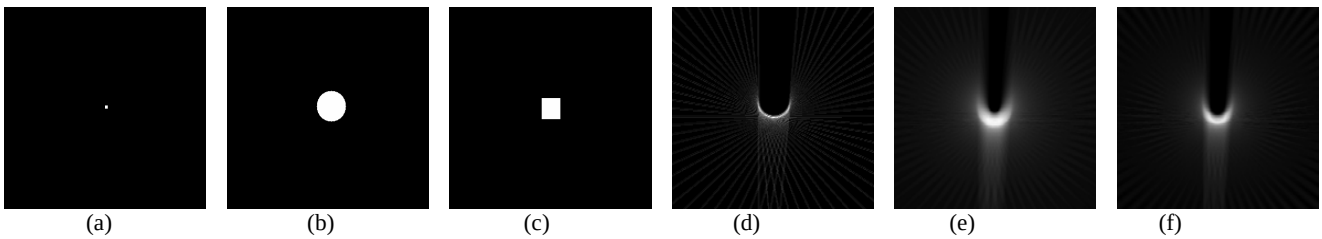

(a) (b) (c) (d) (e) (f)

Fig.1. CT images (central slice) when detector shifts in horizontal transverse direction. The reconstructions of a dot, a circle and a square without misalignment are shown in (a), (b) and (c) respectively. The corresponding images with 10 pixel-offset are shown in (d), (e) and (f).

detector twists around its central column, as shown in Fig.2 (d), the reconstructed images are smaller than those in ideal situation, and the resolution is lower too, though the structure of the images doesn't change. In this situation, seen from the x-ray source, the width of the detector becomes smaller. When the detector skews around the central ray (see Fig.2 (e)), the detected objects are flattened. Under this circumstance, the effective width and height of the detector used in the reconstruction algorithm becomes smaller, which makes the reconstructed images flattened. It leads to the most serious distortion in a CT image.

III. THE CONE-BEAM SCANNER GEOMETRY

A. Aligned geometry

The key components of a cone-beam CT scanner are: an x-ray source, an x-ray planar detector which consists of regularly spaced detector pixels of known size, and a sample turntable located between the source and detector. In an ideal medical cone-beam scanner, typically the object remains fixed but the source and the detector are rotated together. The object is projected onto the planar detector and its projections at different angles are recorded.

In the ideal case, it assumes that the scanner components are perfectly aligned and no error is introduced. Perfect alignment means two conditions must be met. One is the straight line, which is perpendicular to the detector surface passing through its center and contains the focus of the x-ray source (this line is regarded as a central ray, the plane containing the central ray and the central row of the detector is regarded as the mid-plane). The other is the axis of rotation (AOR), which is parallel to the detector and is projected onto the central column of the detector.

To describe the geometry of the ideal scanner, we define a right-handed system of Cartesian coordinates *X*, *Y* and *Z* attached to the planar detector. As shown in Fig.3, plane P denotes the planar detector, the coordinate system origin *O* is

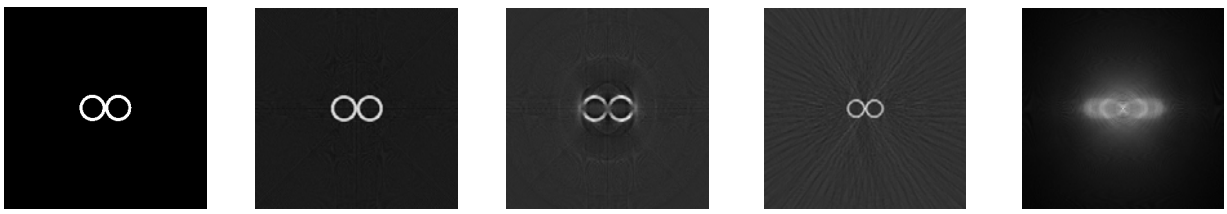

(a) (b) (c) (d) (e)

Fig.2. CT images. (a) Original image in each slice; (b) Image (central slice) without misalignments; (c) Image (the 65th slice from top) when detector tilts $\pi/10$ around its central row, (d) Image (central slice) when detector twist $\pi/4$ around its central column, (e) Image (the 62th slice from top) when detector skews $\pi/7$ around the central ray.

the detector center, the *X* axis points to the ascending column direction, the *Y* axis points to the descending row direction, and the *Z* axis is the normal of the detector and coincident with the central ray. The axis of rotation intersects with the central ray at O_a .

B. Misaligned geometry

In practice, no scanner is free from geometric misalignment. These misalignments can be divided into three parts, including the misalignments of the detector, the misalignments of the x-ray source and the misalignments of the turntable. Case 1 and case 2 describe the deviations of the detector under two different circumstances respectively. It is worth noting that case 1 is a special instance of case 2. Case 3 describes the misalignments of the x-ray source. Case 4 shows the misalignments of the turntable.

Case 1:

Assuming that the source and the turntable are perfectly positioned, it is easy to understand that the deviations of the detector from the ideal position are defined as follows. Fig.4 shows the situation. Among the nine sub-pictures, step 1 to step 6 are the decomposing analyses of the six parameters of the detector. There is not an order of the six parameters in practice.

(1) twist around the central column of the detector by an angle of ϕ degrees, $\phi \in [-\pi/2, \pi/2]$

(2) tilt around the central row of the detector by an angle of θ degrees, $\theta \in [-\pi/2, \pi/2]$

(3) horizontal longitudinal shift along the central ray direction by Δz

(4) horizontal transversal off-center shift along the detector column direction by Δx

(5) vertical off-center shift along the detector row direction by Δy

(6) skew around the central ray by an angle of η degrees, $\eta \in [-\pi/2, \pi/2]$

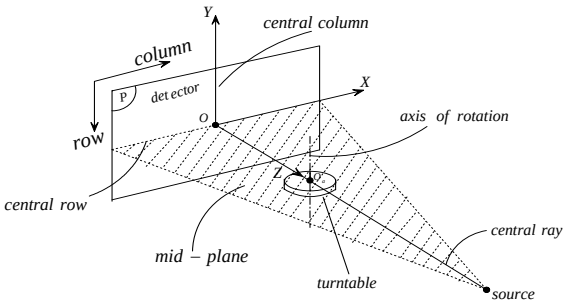

Fig.3. The ideal coordinate system

Case 2:

In practice, the detector can twist around any column, and so do the other five parameters. Therefore the actual deviations of the detector are as follows and the situation is shown in Fig.5. Among the nine sub-pictures, step 1 to step 6 are the decomposing analyses of the six actual parameters of the detector. There is not an order of the six parameters in practice either.

(1) twist around any column of the detector by an angle of ϕ degrees

(2) tilt around any row of the detector by an angle of θ degrees

(3) horizontal longitudinal shift along the central ray direction by Δz

(4) horizontal transversal shift along the detector column direction by Δx

(5) vertical shift along the detector row direction by Δy

(6) skew around the normal of the detector by an angle of η degrees

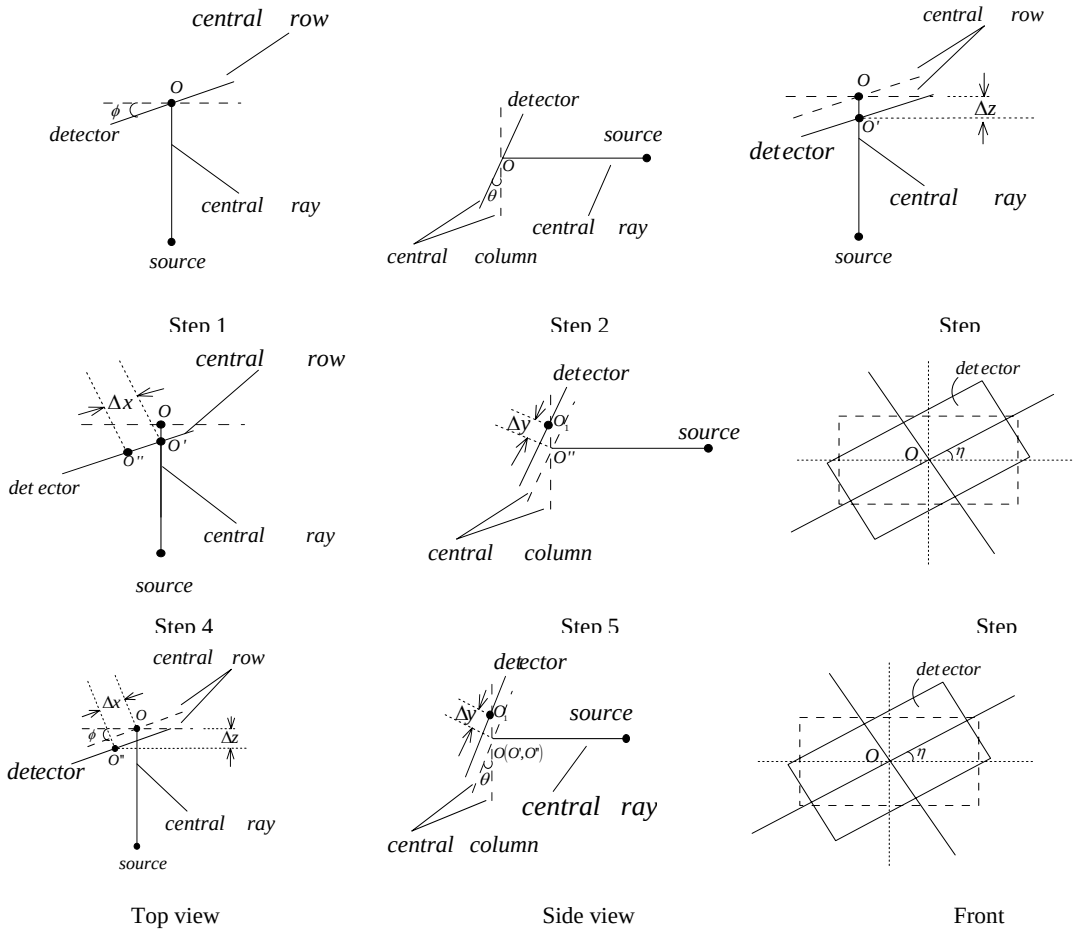

Fig.4. The deviations of the detector from the ideal position.

Because ϕ , θ , η , Δx, Δy and Δz in case 2 can be expressed as the functions of the parameters defined in case 1, case 2 can be converted to case 1. Thus the analysis is simplified.

Case 3:

It is assumed in case 1 and case 2 that the source is perfectly positioned. Sometimes it is not easy for the x-ray source to be perfectly positioned. The deviations of the x-ray source from the ideal position can be categorized as follows and be shown in Fig.6.

(1) vertical shift from the mid-plane by Δy

(2) horizontal transversal shift from the central ray by Δx

(3) horizontal longitudinal shift along the central ray direction by Δz .

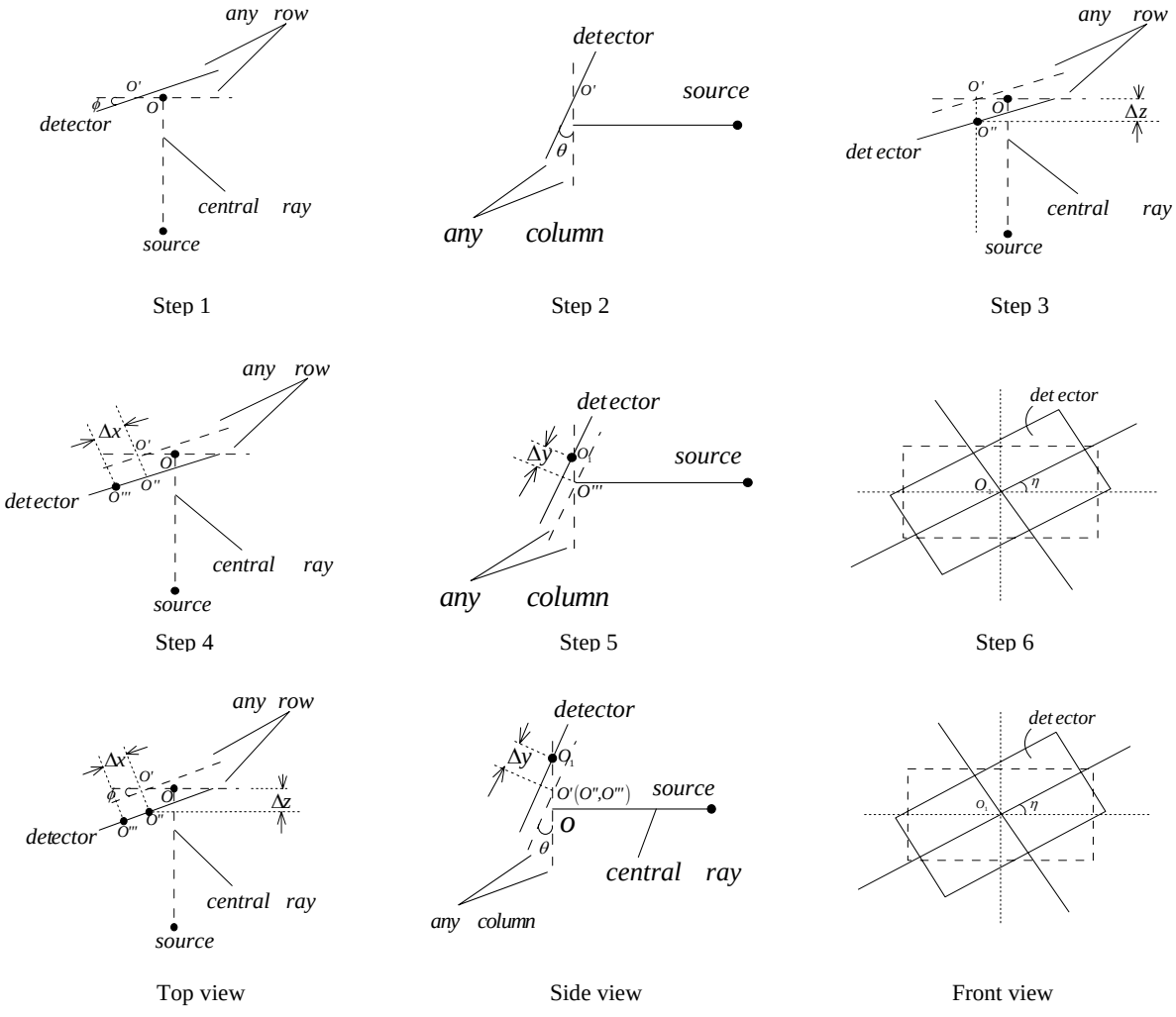

Fig.5. The actual deviations of the detector from the ideal position.

These three deviations also can be expressed as the functions of the parameters defined in case 1. The derivation will be given in appendix A. We should note that the horizontal longitudinal shift of the x-ray source can affect the accuracy of the distance from the x-ray source to the axis of rotation. Thus the inaccurate distance will result in a small error of the calibration result. However, the error is acceptable compared with the actual calibration result.

Case 4:

It is a difficult work to put the turntable at the ideal position, even though we use a level and laser. The four deviations of the turntable can also be converted to the six deviations of the detector introduced in case 1. The derivations in detail will be presented in appendix B. The horizontal longitudinal shift of the turntable will also affect the distance from the x-ray source to the axis of rotation.

Something worthy of note is that the deviations of the source and of the turntable are unavoidable. The equivalent deviations of the detector will still exist even if the detector is well aligned in advance. Since all of the misalignments in case 2, case 3 and case 4 can be equivalent to the six deviations introduced in case 1, we conclude that all of the misaligned errors of the scanner can be converted to the misalignment errors of the detector introduced in case 1, which makes our method have a more robust adaptation without loss of generality. Therefore we can concentrate on the calibration of the six misalignment parameters in case 1. Based on this analysis, our method tries to avoid any assumption about the six misalignment parameters of the detector in advance.

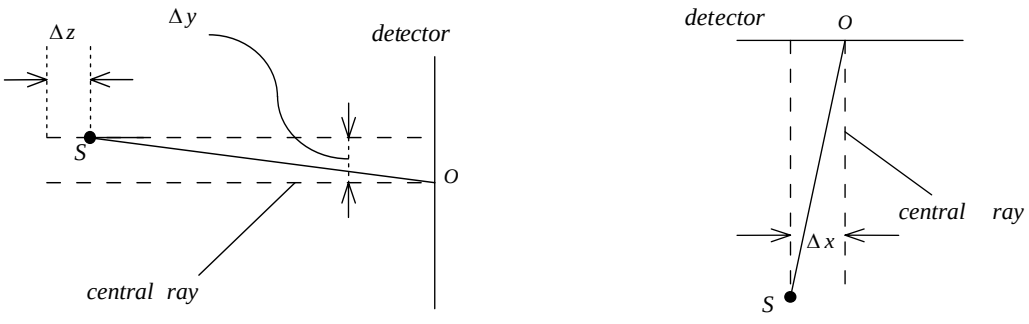

Fig.6. The deviations of the x-ray source from the ideal position.

IV. ANALYTIC CALIBRATION

A. Principles

There are seven parameters totally to describe the scanner geometry, including error of the distance from x-ray source to axis of rotation and the six parameters of the detector (ϕ , θ , η , Δx , Δy , Δz). As proved in appendix A, the error of the distance from x-ray source to axis of rotation can be converted to Δz of the detector. The purpose of our method is to derive the analytic expressions of the six unknown scanner parameters (ϕ , θ , η , Δx , Δy , Δz) according to the simple projection of a phantom collected at only one angle. It is expected that the parameters of the scanner should be separated, and the analytic expressions contain as few independent parameters as possible.

The scanner calibration is carried out in three steps. We first place the turntable in the position as ideal as possible with the usual methods. It is obvious that there is still some small unavoidable misalignment. Then we use the scanner to collect a cone-beam projection of a calibration phantom as shown in fig.7, which is composed of four points. The four points are placed at the vertexes of a square respectively. We also need to measure the length of one side of the square on the calibration phantom accurately. In the ideal case, the projections of four such points are still on the vertexes of a square on the detector, as shown in Fig.8 (for convenience, we just keep the four point objects on the phantom and omit other parts of the phantom), where L denotes the length of the side of the ideal projection square $AA'B'B$ on plane P. L can be calculated according to the distance f from the source to the axis of rotation, the distance d from the source to the detector, and the length of the side of the square on the calibration phantom. Since the deviation of distance f can be converted to that of distance d , and the deviation of distance d is one of the parameters we want to calibrate, we only need to know l in advance.

In the second step, according to the center coordinates of the four projected points calculated, we can compute the lengths of four sides of the projected quadrangle on the misaligned detector in case 1. Fig.9 shows the situation. The analytic expressions are derived which show that the ratio of the left side to the right side of the projected quadrangle can be expressed as the function of angle ϕ , which can then be calculated using this function containing only this unknown parameter. In the same way, the ratio of the upper side to the lower side of the projected quadrangle can be expressed as the function of angle θ , which can also be solved from this equation containing only one unknown

parameter. Then ϕ and θ can be separated from complex situations and can be expressed as the functions of the ratio of lengths of

sides respectively. Thus the computational complexity is reduced greatly. Δz also can be computed from any one of the lengths of the four sides after calibrating the angle ϕ and angle θ .

In the third step, to compute Δx , Δy and angle η , we need to calculate the center coordinate of one point projection on the detector that has been twisted and tilted. According to the angle ϕ, θ and Δz computed above and the information acquired in this step, we can calculate the skewed angle η , and consequently compute Δx and Δy . The details will be described in parts B, C and D.

B. Calculation of ϕ, θ

Similar to the coordinate system X ,Y and Z introduced in Fig.3, we define another two right-handed systems of Cartesian coordinates to describe the misalignments of the scanner in case 1, which are shown in Fig.10 and Fig.11 respectively. One is X_1, Y_1 and Z_1 attached to the plane (P_1) which denotes the ideal detector plane twisted with angle ϕ around the Y axis. The other is X_2, Y_2 and Z_2 attached to the plane (P_2) which denotes the P_1 tilted angle θ around

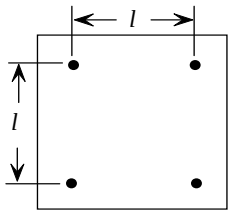

Fig.7. Calibration phantom

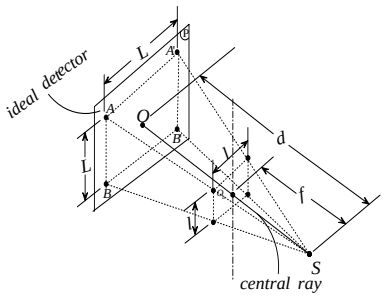

Fig.8. The ideal scanner assumed in our method

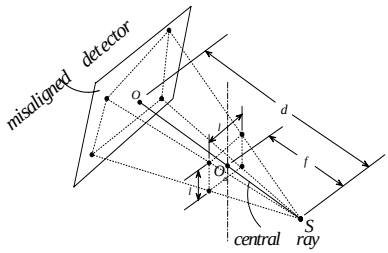

Fig.9. The misaligned scanner

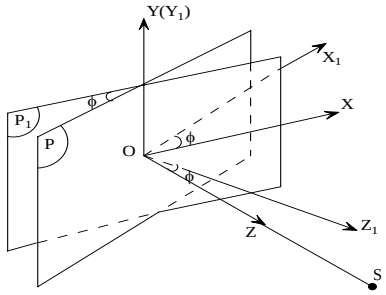

Fig.10. The relationship between P and P_1

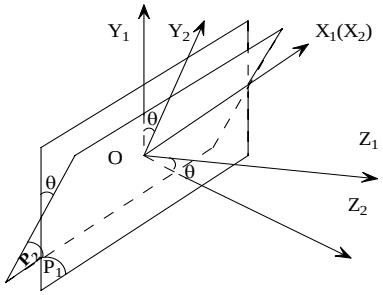

Fig.11. The relationship between P_1 and P_2

the X_1 axis. Point O is still the origin of these two coordinate systems. The X_1 axis points in the ascending column direction, the Y_1 axis is coincident with the Y axis, and the Z_1 axis is the normal of P_1. The angle between the X axis and the X_1 axis is ϕ , equal to the one between the Z axis and the Z_1 axis. The X_2 axis is coincident with the X_1 axis, the Y_2 axis is perpendicular to the detector rows and points in the descending row direction, and the Z_2 axis is the normal of P_2. The angle between the Y_1 axis and the Y_2 axis is θ equal to the one between the Z_1 axis and the Z_2 axis.

Based on the analysis of the relationship between the lengths of sides of the projection square on the misaligned detector and the misalignment parameters, we find that the ratio of one side to its opposite side of the projected quadrangle are relevant to the twisted angle and tilted angle, but irrelevant to the other four misalignment parameters. Therefore we simplify the figure as shown in Fig.12 (Assumed $\Delta x = 0, \Delta y = 0, \Delta z = 0, \eta = 0$).

In Fig.12, point S is the x-ray source, the square $AA'B'B$ on plane P is the ideal projection of the four points on the calibration phantom. When plane P twists angle ϕ to plane P_1, the projection of the four points is the quadrangle $DD'C'C$.

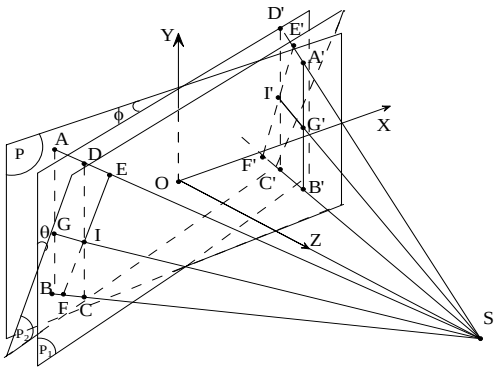

Fig.12. Front view (seen from the x-ray source).

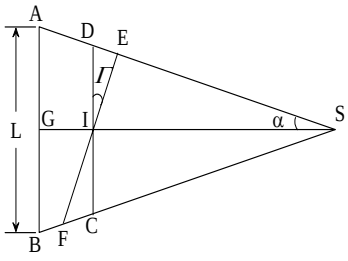

Fig.13. Side view

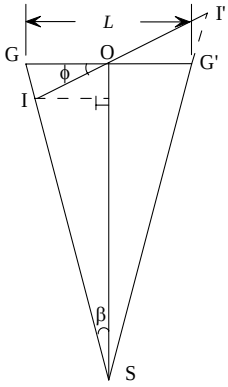

Fig.14. Top view

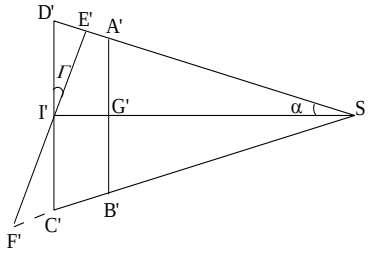

Fig.15. Side view

Then with plane P_1 tilting angle θ to plane P_2, the quadrangle $DD'C'C$ is changed into $EE'F'F$. Points G, G', I' and I are the midpoints of AB, $A'B'$, DC and $D'C'$ respectively.

As shown in Fig.13 and Fig.14, the angle between *DC* and *EF* is Γ, which can be expressed as the function of θ. The angle between *IO* and *GO* is ϕ. α denotes the angle between *AS* and *GS*, which is equal to the one between *BS* and *GS*. β denotes the angle between *GS* and *SO*.

In Fig.14 and Fig.15, the angles between $D'C'$ and $E'F'$, $I'O$ and $G'O$, $A'S$ and $G'S$, $G'S$ and SO are Γ, ϕ, α and β respectively. We have:

$$L = l \cdot d / f \tag{1}$$

$$GS = \sqrt{(L/2)^2 + d^2} \tag{2}$$

According to the sine law:

$$S_{\Delta SEI} = \frac{1}{2} \cdot ES \cdot EI \cdot \sin(\angle FES) = \frac{1}{2} \cdot EI \cdot SI \cdot \sin(\angle EIS) \tag{3}$$

$$S_{\Delta SEF} = \frac{1}{2} \cdot FS \cdot ES \cdot \sin(\angle ASB) = \frac{1}{2} \cdot EF \cdot FS \cdot \sin(\angle EFS) \tag{4}$$

Where:

$$\angle FES = \pi/2 + \Gamma - \alpha \tag{5}$$

$$\angle EIS = \pi/2 - \Gamma \tag{6}$$

$$\angle ASB = 2\alpha \tag{7}$$

$$\angle EFS = \pi/2 - \Gamma - \alpha \tag{8}$$

$$\tan\alpha = \frac{AG}{GS} = \frac{L/2}{\sqrt{(L/2)^2 + d^2}} \tag{9}$$

The relationship between Γ and θ is shown in Fig.16. DM is the normal of plane P_2 containing point D, then we know $DM \perp IM$, where *M* is the intersection of the normal and plane P_2. If we assume that MN is perpendicular to EI and the intersection is N, then DN must be perpendicular to EI and the intersection is N.

Since:

$$\angle DIM = \theta \tag{10}$$

$$\angle DIE = \Gamma \tag{11}$$

If we define:

$$\angle MIN = \angle MIE = \gamma \tag{12}$$

Then we will get:

$$\cos \Gamma = \frac{IN}{DI} = \frac{IN}{MI} \cdot \frac{MI}{DI} = \cos\gamma \cdot \cos\theta \tag{13}$$

Where:

$$\cos\gamma = \cos(\pi/2 - \angle EIO) = \sin(\angle EIO) \tag{14}$$

$$\cos(\angle EIO) = \frac{(OI^2 + EI^2 - OE^2)}{2 \cdot OI \cdot EI} \tag{15}$$

Since:

$$\tan\beta = \frac{OI \cdot \cos\phi}{SO - OI \cdot \sin\phi} = \frac{OI \cdot \cos\phi}{d - OI \cdot \sin\phi} = \frac{(L/2)}{d} \quad (\text{See Fig.14}) \tag{16}$$

Therefore:

$$OI = \frac{L/2 \cdot d}{d \cdot \cos\phi + L/2 \cdot \sin\phi} \tag{17}$$

$$SI = \frac{OI \cdot \cos\phi}{\sin\beta} = \frac{d \cdot \sqrt{(L/2)^2 + d^2}}{(d + L/2 \cdot \tan\phi)} \tag{18}$$

$$ES = \frac{SI \cdot \cos\Gamma}{\cos(\alpha - \Gamma)} \tag{19}$$

$$OE = \sqrt{ES^2 + d^2 - 2 \cdot d \cdot ES \cdot \cos\alpha \cdot \cos\beta} \tag{20}$$

$$EI = \sqrt{ES^2 + SI^2 - 2ES \cdot SI \cdot \cos\alpha} \tag{21}$$

Combining (3) and (4) we get:

$$\begin{aligned} EF &= \frac{ES \cdot \sin(2\alpha)}{\cos(\alpha + \Gamma)} = \frac{SI \cdot \cos\Gamma \cdot \sin(2\alpha)}{\cos(\alpha + \Gamma) \cdot \cos(\alpha - \Gamma)} \\ &= \frac{d \cdot \sqrt{L^2 + 4d^2} \cdot \cos\Gamma \cdot \sin(2\alpha)}{(2d + L \cdot \tan\phi) \cdot \cos(\alpha + \Gamma) \cdot \cos(\alpha - \Gamma)} \end{aligned} \tag{22}$$

Similar to the method used above, we get:

$$E'F' = \frac{E'S \cdot \sin(2\alpha)}{\cos(\alpha+\Gamma)} = \frac{SI' \cdot \cos\Gamma \cdot \sin(2\alpha)}{\cos(\alpha+\Gamma)\cdot\cos(\alpha-\Gamma)} = \frac{d \cdot \sqrt{L^2+4d^2} \cdot \cos\Gamma \cdot \sin(2\alpha)}{(2d - L\cdot\tan\phi)\cdot\cos(\alpha+\Gamma)\cdot\cos(\alpha-\Gamma)} \quad (23)$$

The derivation of $E'F'$ in detail can be found in appendix C.

Combining (22) and (23), we get such a relationship between EF and $E'F'$:

$$\frac{EF}{E'F'} = \frac{2d - L\cdot\tan\phi}{2d + L\cdot\tan\phi} = \frac{2f - l\cdot\tan\phi}{2f + l\cdot\tan\phi} \quad (24)$$

In the same way we can get:

$$\frac{EE'}{FF'} = \frac{\sqrt{L^2+4d^2} - L\cdot\tan\Gamma}{\sqrt{L^2+4d^2} + L\cdot\tan\Gamma} = \frac{\sqrt{l^2+4f^2} - l\cdot\tan\Gamma}{\sqrt{l^2+4f^2} + l\cdot\tan\Gamma} \quad (25)$$

The derivation of formula (25) in detail can also be found in the appendix C.

The formulae (24) and (25) are very important results in our calibration method. Since length of side l of the square on the calibration phantom is a constant, and so is the distance f, angle ϕ and Γ then can be calculated easily. Though it is impossible to align the distance f exactly in practice, the misalignment of it can be converted to the horizontal longitudinal shift (Δz) of the detector, as described in appendix A and B. Later, the angle θ can be derived using formulae (10)–(21). During this step, the lengths of EF, $E'F'$, EE' and FF' need to be calculated according to the locations of E, E', F, F' in advance.

C. Calculation of Δz

We assume that the misaligned detector moves a distance about Δz along the Z axis. Then, the distance from the source to the detector in (22) will be displaced by $(d+\Delta z)$. So we have:

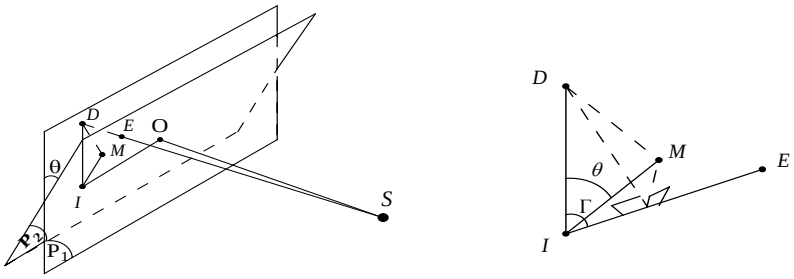

Fig.16 The relationship between Γ and θ

$$EF = \frac{(d+\Delta z)\cdot\sqrt{L^2+4(d+\Delta z)^2}\cdot\cos\Gamma\cdot\sin(2\alpha)}{[2\cdot(d+\Delta z)+L\cdot\tan\phi]\cdot\cos(\alpha+\Gamma)\cdot\cos(\alpha-\Gamma)} \quad (26)$$

$$L = l\cdot\frac{d+\Delta z}{f} \quad (27)$$

Because the length of EF, angle ϕ and Γ have been calculated, then the moved distance Δz can be acquired using (26) and (27).

D. Calculation of $\eta, \Delta x, \Delta y$

To explain the calibration method clearly, we define two orthogonal systems of Cartesian coordinates. One is X_3 and Y_3 (shown in Fig.17), which denotes plane P_2 moving a distance about Δx along X_2 axis and a distance about Δy along Y_2 axis respectively to plane P_3, and the origin of this coordinate system is O_1. The other is X_4 and Y_4 (shown in Fig.18), which denotes the X_3 and Y_3 skewing angle η, and O_1 is still the origin.

From the above two figures, we know:

$$x_3 = x_2 - \Delta x \quad (28)$$

$$y_3 = y_2 - \Delta y \quad (29)$$

$$x_4 = x_3\cdot\cos\eta + y_3\cdot\sin\eta \quad (30)$$

$$y_4 = -x_3\cdot\sin\eta + y_3\cdot\cos\eta \quad (31)$$

If we define Δx_1 as the difference between the abscissa of one projected point on plane P_4 and that on plane P_2, we can define Δy_1 as the difference between the ordinate of the projected point on plane P_4 and that on plane P_2, then we have:

$$\Delta x_1 = x_4 - x_2 = \Delta x\cdot\cos\eta + \Delta y\cdot\sin\eta \quad (32)$$

$$\Delta y_1 = y_4 - y_2 = -\Delta x\cdot\sin\eta + \Delta y\cdot\cos\eta \quad (33)$$

Combing formula (28)–(33), we get:

$$\begin{aligned} x_4 &= x_2\cdot\cos\eta + y_2\cdot\sin\eta - (\Delta x\cdot\cos\eta + \Delta y\cdot\sin\eta) \\ &= x_2\cdot\cos\eta + y_2\cdot\sin\eta - \Delta x_1 \end{aligned} \quad (34)$$

$$\begin{aligned} y_4 &= -x_2\cdot\sin\eta + y_2\cdot\cos\eta - (-\Delta x\cdot\sin\eta + \Delta y\cdot\cos\eta) \\ &= -x_2\cdot\sin\eta + y_2\cdot\cos\eta - \Delta y_1 \end{aligned} \quad (35)$$

If we define (x_4, y_4) as the center coordinate of any one of the four projection points on the misaligned detector (P_4). Then the line passing through this projection point and the source will intersect with plane P_2, and the center coordinate

of the intersection is defined as (x_2, y_2). It is easy to calculate these coordinates according to formula (36)-(38). The deviation is given in appendix C. Then we have:

$$x_2 = -OI/2 + (EI^2 - OE^2)/(2 \cdot OI) \tag{36}$$

$$y_2 = \sqrt{EI^2 - (OI + x_2)^2} \tag{37}$$

or $$y_2 = -\sqrt{EI^2 - (OI + x_2)^2} \tag{38}$$

If we take one of the upper two points on the phantom as the reference, then y_2 will be computed using formula (37). Otherwise y_2 will be computed using formula (38). Then we can calculate angle η according to (34)-(35) and compute Δx and Δy in succession using (32) and (33).

V. SIMULATING RESULTS

As shown in Fig.19, the whole procedure of calibration includes eight steps. All of the symbols shown in the figure have been introduced in section III.

The main parameters of typical scanner geometry in the simulation study are as follows:

(1) A two-dimensional detector with 576 × 768 elements of $(0.1458\text{mm})^2$ size each.

(2) The distance f from the x-ray source to the axis of rotation is 350mm.

(3) The distance d from the x-ray source to the detector is 500mm.

(4) The length of side on the calibration phantom l is 40mm.

We have simulated different misalignments of the x-ray source, the turntable and the detector when the coordinates of

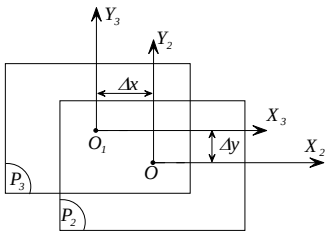

Fig.17. Relationship between P_2 and P_3

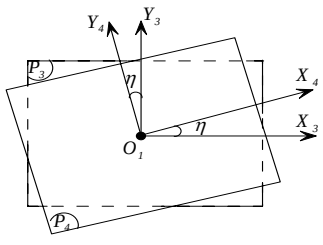

Fig.18. Relationship between P_3 and P_4.

the four projected points are measured accurately, results being listed in table 1. We find that there are small differences between the misalignments computed by our method and those equivalent results. Compared with equivalent results, the differences are very small. These differences are caused by the inaccurate distance f used in formula (24) and (25).

We also simulated the influence of accuracy of the center coordinates on the results. This experiment was done under such circumstance that there are only misalignments of the detector. The results are listed in table 2.From table 2, we find that the uncertainty of the scanner parameters depends on the accuracy to which the coordinates of the four points on the misaligned detector can be estimated. When the center coordinates are exactly known, the analytic calibration method proposed in this paper will provide exact results. With the measurement error increasing, the difference between the true value and the actual value becomes more obvious. From table 2 we also find that the deviations of ϕ and θ are more serious than those of Δx , Δy , Δz and η . The reason for the phenomenon is that a small error of the coordinates will result in a small deviation of the length of the side. Since the tangent functions of angle ϕ and Γ are the linear functions of the length of the side, as presented in formulae (24) and (25), and the cosine function of angle θ can be expressed as the function of angle Γ as introduced in formula (13), then a small deviation will affect the angle ϕ and θ greatly. Combining formulae (34) and (35), the sine function of angle η is expressed as the function of the length of the side. Compared with the variation of a tangent function, the variation of a sine function is gentle, then angle η is affected less by the small deviation of the length of the side. Because Δx , Δy , Δz can be expressed as the linear function of the length of the side, referring to formulae (26),(32),(33),the three parameters are also affected less by the deviation. As presented in section Ⅱ, even the uncertainties of ϕ and θ are more serious than those of the other four parameters, the artifacts caused by them are less. Fortunately,

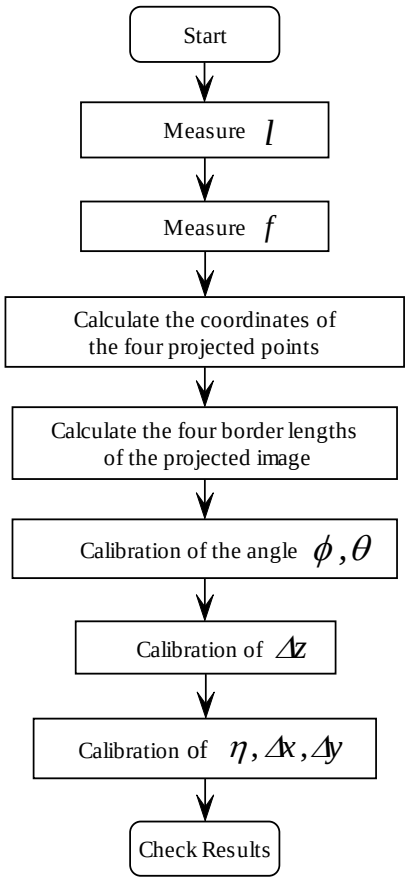

Fig.19. Flow Chat for calibrating misaligned scanner using a four-point phantom

the calibration of Δx , Δy , Δz and η are fairly accurate using our method. Since random noise and scatter always exist in practice, the error on the calculation of the center coordinate is unavoidable. To reduce the effects caused by random noise and scatter, we need to collect the projections at one position many times and average the calibration results. Table 3 presents the calibration result when the error of the measured coordinates is one-pixel. Taking the third row in the table as an example, the first column denotes the error of center coordinates of points E, E', F, F', which means the row coordinate of point E decreases one pixel while other coordinates are accurate. At the same time, the next six columns show the calibration results under such a situation when not all coordinates are accurate.

Table 1. Simulating results

Misalignments of the source	Δx (mm)	1	0	0	1	1	0	1
	Δy (mm)	1	0	0	1	1	0	1
	Δz (mm)	10	0	0	10	10	0	10
Misalignments of the turntable (no order)	Δx (mm)	0	1	0	1	0	1	1
	Δz (mm)	0	1	0	1	0	1	1
	θ (deg)	0	5	0	5	0	5	5
	η (deg)	0	5	0	5	0	5	5
Misalignments of the detector (no order)	Δx (mm)	0	0	1	0	1	1	1
	Δy (mm)	0	0	1	0	1	1	1
	Δz (mm)	0	0	10	0	10	10	10
	ϕ (deg)	0	0	5	0	5	5	5
	θ (deg)	0	0	5	0	5	5	5
	η (deg)	0	0	5	0	5	5	5
Equivalent misalignments of the detector (as shown in case 1)	Δx (mm)	0.4286	1.4286	1	1.8452	1.4286	2.5119	2.9286
	Δy (mm)	0.4286	0	1	0.4286	1.4286	0.9090	1.3376
	Δz (mm)	4.1667	-14.7059	10	2.7459	14.1667	8.5673	12.7459
	ϕ (deg)	0	0	5	0	5	5	5
	θ (deg)	0	-2.7258	5	-2.7258	4.6072	2.1460	2.0060
	η (deg)	0	0	5	5	5	10	10
Misalignments of the detector computed by our method (as shown in case 1)	Δx (mm)	0.4286	1.4286	1	1.8452	1.4286	2.5119	2.9286
	Δy (mm)	0.4286	0	1	0.4286	1.4286	0.9090	1.3376
	Δz (mm)	4.1806	-14.7394	10	2.7520	14.2987	8.5666	12.7459
	ϕ (deg)	0	0	5	0	5.1408	5.0852	5.1267
	θ (deg)	0	-2.7089	5	-2.7277	4.9226	2.0667	1.7648
	η (deg)	0	0	5	5	5	10	10

Table 2. Simulating results

	ϕ (deg)	θ (deg)	η (deg)	Δx (mm)	Δy (mm)	Δz (mm)
True value	5	5	5	1	1	10
No error	5.0000	5.0000	5.0000	1.0000	1.0000	10.0000
Error of 1/10 pixel	4.9966	4.9966	5.0001	1.0000	1.0000	10.0000
Error of 3/10 pixel	4.9698	4.9697	5.0000	1.0000	1.0000	10.0000
Error of 1/2 pixel	4.9173	4.7445	4.9994	0.9999	1.0000	10.0000
Error of 1 pixel	4.6754	5.3798	5.0001	0.9999	0.9999	10.0000

Table 3. Uncertainties of the scanner parameters when the error of the measured coordinates is one-pixel

Errors of the center coordinates of E, E', F, F' (pixel)	ϕ **(deg)**	θ **(deg)**	η **(deg)**	Δx **(mm)**	Δy **(mm)**	Δz **(mm)**
(0,0) (0,0)(0,0) (0,0)	5	5	5	1	1	10
(-1,0) (0,0)(0,0) (0,0)	-12.0212	3.4400	4.9088	1.0016	0.9984	10.0000
(0,-1) (0,0)(0,0) (0,0)	6.3112	-12.0164	3.9458	1.0182	0.9814	10.0000
(1,0) (0,0)(0,0) (0,0)	21.3403	6.3957	5.0948	0.9983	1.0016	10.0000
(0,1) (0,0)(0,0) (0,0)	3.5250	21.3357	6.0706	0.9811	1.0185	10.0000
(0,0) (-1,0)(0,0) (0,0)	21.1653	6.3957	4.9089	1.0016	0.9984	10.0000
(0,0) (0,-1)(0,0) (0,0)	3.7327	21.3357	3.9289	1.0185	0.9811	10.0000
(0,0) (1,0)(0,0) (0,0)	-12.1322	3.4400	5.0944	0.9983	1.0016	10.0000
(0,0) (0,1)(0,0) (0,0)	6.4189	-12.0164	6.0482	0.9815	1.0181	10.0000
(0,0) (0,0)(-1,0) (0,0)	21.3403	6.9535	5.0944	0.9983	1.0016	10.0000
(0,0) (0,0)(0,-1) (0,0)	3.5250	21.1544	6.0482	0.9815	1.0181	10.0000
(0,0) (0,0)(1,0) (0,0)	-12.0212	3.5560	4.9089	1.0016	0.9984	10.0000
(0,0) (0,0)(0,1) (0,0)	6.3112	-12.1197	3.9289	1.0185	0.9811	10.0000
(0,0) (0,0)(0,0) (-1,0)	-12.1322	3.5560	5.0943	0.9983	1.0016	10.0000
(0,0) (0,0)(0,0) (0,-1)	6.4189	-12.1197	6.0648	0.9812	1.0184	10.0000
(0,0) (0,0)(0,0) (1,0)	21.1653	6.5935	4.9093	1.0016	0.9984	10.0000
(0,0) (0,0)(0,0) (0,1)	3.7327	21.1544	3.9514	1.0184	0.9815	10.0000
(-1,-1) (0,0)(0,0) (0,0)	-10.7721	-13.4812	3.8750	1.0194	0.9802	10.0000
(-1,1) (0,0)(0,0) (0,0)	-13.4067	19.9363	5.9581	0.9831	1.0166	10.0000
(1,-1) (0,0)(0,0) (0,0)	22.5012	10.6862	4.0194	1.0170	0.9827	10.0000
(1,1) (0,0)(0,0) (0,0)	20.0177	22.5711	6.1877	0.9791	1.0205	10.0000
(0,0) (-1,-1)(0,0) (0,0)	20.0690	22.5711	3.8559	1.0198	0.9798	10.0000
(0,0) (-1,1)(0,0) (0,0)	22.3787	-10.6862	5.9402	0.9835	1.0163	10.0000
(0,0) (1,-1)(0,0) (0,0)	-13.3675	19.9364	4.0047	1.0172	0.9825	10.0000
(0,0) (1,1)(0,0) (0,0)	-10.7296	-13.4812	6.1600	0.9795	1.0200	10.0000
(0,0) (0,0)(-1,-1) (0,0)	20.0177	22.5163	6.1600	0.9795	1.0200	10.0000
(0,0) (0,0)(-1,1) (0,0)	22.0512	-10.5430	4.0047	1.0172	0.9825	10.0000
(0,0) (0,0)(1,-1) (0,0)	-13.4067	19.9042	5.9402	0.9835	1.0163	10.0000
(0,0) (0,0)(1,1) (0,0)	-10.7721	-13.5260	3.8559	1.0198	0.9798	10.0000
(0,0) (0,0)(0,0) (-1,-1)	-10.7296	-13.5260	6.1811	0.9792	1.0204	10.0000
(0,0) (0,0)(0,0) (-1,1)	-13.3675	19.9042	4.0246	1.0169	0.9828	10.0000
(0,0) (0,0)(0,0) (1,-1)	22.3787	-10.5430	5.9530	0.9832	1.0165	10.0000
(0,0) (0,0)(0,0) (1,1)	20.0690	22.5163	3.8808	1.0193	0.9803	10.0000
Average value	4.6754	5.3798	5.0001	0.9999	0.9999	10.0000

VI. CONCLUSION

In this paper, a new method for alignment of x-ray cone-beam CT system is suggested. Our approach allows us to measure only one projection to estimate all the parameters that totally describe the scanner geometry, by using a four-point phantom. In addition, there is no restriction on any one of parameters. Compared with other calibration methods, it estimates a set of parameters using analytical formulae. Therefore, it will not fall into the trouble of a local minima. In addition, this method doesn't need projections at multi angles, which avoids introducing errors during the

rotation. Furthermore, there is no assumption on the accuracy of any one of the six parameters in advance. The accuracy of this method is confirmed by the simulated results. It is proved that this method is applicable and efficient for misaligned scanner geometry.

The uncertainty of the scanner parameters depends on the accuracy to which the centroid of the E , F , E' , F' can be estimated. Thus the ball should be projected on a large number of pixels, and the selection of phantom material must be considered [8]. We can also use a steel plate drilled with four apertures as the phantom, which should be thin to minimize the effects of the attenuation of the x-ray beam by the borders of the aperture. The only expense is that the calibration point object should be placed with known relative positions. The design of this calibration object is not very difficult. Correction in reconstruction will be described in forthcoming papers.

APPENDIX A

Deviation 1: If the source has a vertical shift from the mid plane by Δy_1, as shown in Fig.20, then this shift can be converted to Δy of the detector using formula (A1)~(A2).

Since: $$\frac{\Delta y}{\Delta y_1} = \frac{d - f}{f} \tag{A1}$$

So: $$\Delta y_1 = \frac{f \cdot \Delta y}{d - f} \tag{A2}$$

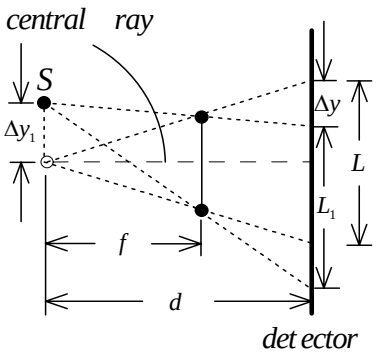

Fig. 20 Vertical shift of the source

Deviation 2: If the source has a horizontal transversal shift from the central ray by Δx_1, as shown in Fig.21, then this shift can be converted to Δx of the detector using formula (A3)~(A4).

Since: $$\frac{\Delta x}{\Delta x_1} = \frac{d-f}{f} \tag{A3}$$

So: $$\Delta x_1 = \frac{f \cdot \Delta x}{d-f} \tag{A4}$$

Deviation 3: If the source has a horizontal longitudinal shift from the central ray by Δz_1, as shown in Fig.22, then this shift can be converted to Δz of the detector using formula (A5)~(A6). Here l is the length side of the square on the calibration phantom.

Since: $$\frac{f-\Delta z_1}{d-\Delta z_1} = \frac{l}{L_3} = \frac{f}{d+\Delta z} \tag{A5}$$

So: $$\Delta z_1 = \frac{f \cdot \Delta z}{d-f+\Delta z} \tag{A6}$$

APPENDIX B

Deviation 1: If the turntable has a horizontal longitudinal shift along the central ray direction by Δz_2, as shown in Fig.23, then this shift can be converted to Δz of the detector using formula (B1)~(B2). Here l is the length side of the square on the calibration phantom.

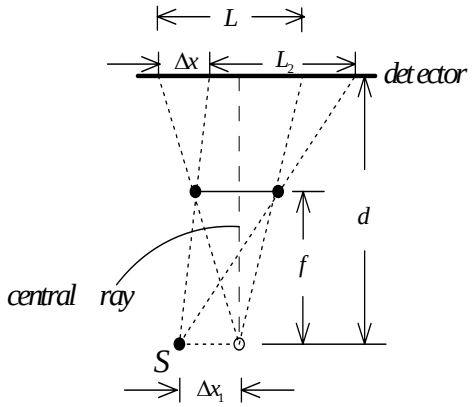

Fig.21 Horizontal transversal shift of the source

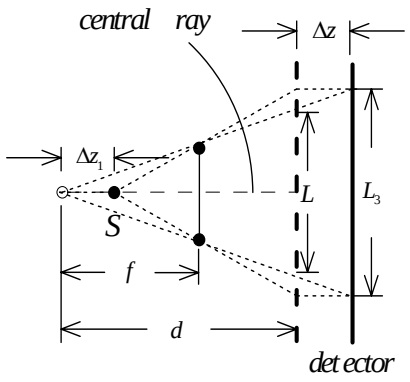

Fig.22 Horizontal longitudinal shift of the source

Since: $$\frac{f-\Delta z_2}{d}=\frac{l}{L_4}=\frac{f}{d+\Delta z} \tag{B1}$$

So: $$\Delta z_2=\frac{f\cdot\Delta z}{d+\Delta z} \tag{B2}$$

Deviation 2: If the turntable has a horizontal transversal shift along the central ray direction by Δx_2, as shown in Fig.24, then this shift can be converted to Δx of the detector using formula (B3)~(B4).

Since: $$\frac{\Delta x_2}{\Delta x}=\frac{f}{d} \tag{B3}$$

So: $$\Delta x_2=\frac{f}{d}\cdot\Delta x \tag{B4}$$

Deviation 3: If the turntable has a tilt around the ideal axis of rotation by an angle θ_1, as shown in Fig.25, then this tilt can be converted to θ of the detector and the horizontal longitudinal shift Δz of the detector using formula (B7)~(B9). Here l is the length side of the square on the calibration phantom.

Since:

$$\frac{L_6\cdot\cos\theta}{l/2}=\frac{d-\Delta z+L_6\cdot\sin\theta}{f} \tag{B5}$$

$$\frac{\frac{l}{2}\cdot\cos\theta_1}{L_6}=\frac{f-\frac{l}{2}\cdot\sin\theta_1}{d} \tag{B6}$$

So: $$\frac{d\cdot\cos\theta_1}{f-\frac{l}{2}\cdot\sin\theta_1}=\frac{d-\Delta z}{f\cdot\cos\theta-\frac{l}{2}\cdot\sin\theta} \tag{B7}$$

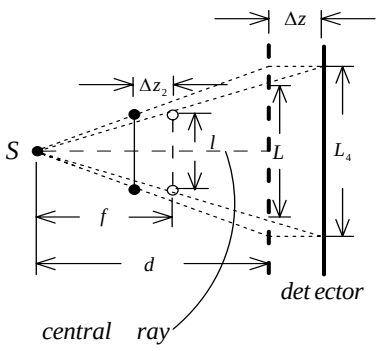

Fig. 23 Horizontal longitudinal shift of the turntable

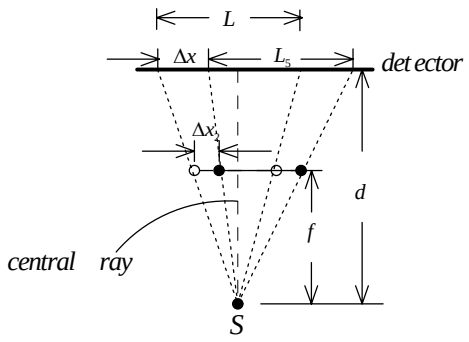

Fig. 24 Horizontal transversal shift of the turntable

Also we have:
$$\frac{\frac{d\cdot\sin\alpha}{\cos(\alpha-\theta)}}{L_6}=\frac{d}{d-\Delta z} \tag{B8}$$

Here:
$$\tan\alpha=\frac{l/2}{f} \tag{B9}$$

Deviation 4: If the turntable has a skew around the ideal axis of rotation by an angle η_1, as shown in Fig.26, then this tilt can be converted to η of the detector using formula (B10).

$$\eta_1=\eta \tag{B10}$$

APPENDIX C

We derive formula (23), (24), (25), in part B section Ⅳ and formula (35), (36), (37) in part D section Ⅳ as follows. As shown in Fig.14 and Fig.15, we have:

$$SI'=\frac{d\cdot G'S}{d-L/2\cdot\tan\phi} \tag{C1}$$

$$G'S=\sqrt{(L/2)^2+d^2} \tag{C2}$$

According to the sine law:

$$S_{\Delta SE'I'}=\frac{1}{2}\cdot E'S\cdot E'I'\cdot\sin(\angle F'E'S)=\frac{1}{2}\cdot E'I'\cdot SI'\cdot\sin(\angle E'I'S) \tag{C3}$$

$$\begin{aligned}S_{\Delta SE'F'}&=\frac{1}{2}\cdot F'S\cdot E'S\cdot\sin(\angle A'SB')\\&=\frac{1}{2}\cdot E'F'\cdot F'S\cdot\sin(\angle E'F'S)\end{aligned} \tag{C4}$$

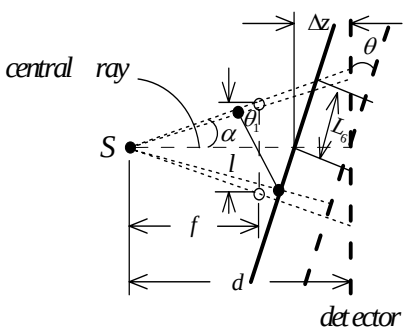

Fig. 25 Tilt of the turntable

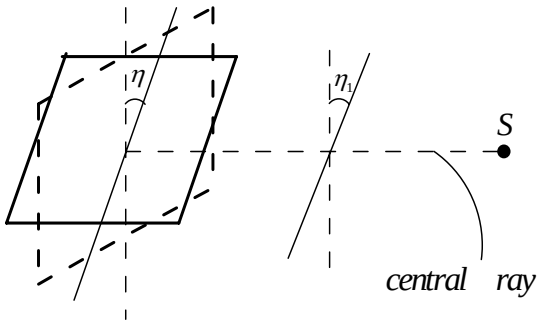

Fig.26 Skew of the turntable

Where:

$$\angle F'E'S = \pi/2 + \Gamma - \alpha \tag{C5}$$

$$\angle E'I'S = \pi/2 - \Gamma \tag{C6}$$

$$\angle A'SB' = 2\alpha \tag{C7}$$

$$\angle E'F'S = \pi/2 - \Gamma - \alpha \tag{C8}$$

Combining (C3) and (C4) we can get:

$$\begin{aligned} E'F' &= \frac{E'S \cdot \sin(2\alpha)}{\cos(\alpha+\Gamma)} = \frac{SI' \cdot \cos\Gamma \cdot \sin(2\alpha)}{\cos(\alpha+\Gamma)\cdot\cos(\alpha-\Gamma)} \\ &= \frac{d \cdot \sqrt{L^2+4d^2} \cdot \cos\Gamma \cdot \sin(2\alpha)}{(2d - L\cdot\tan\phi)\cdot\cos(\alpha+\Gamma)\cdot\cos(\alpha-\Gamma)} \end{aligned} \tag{23}$$

Combining (17) and (18), we can get such a relationship between *EF* and *E'F'*:

$$\frac{EF}{E'F'} = \frac{2d - L\cdot\tan\phi}{2d + L\cdot\tan\phi} = \frac{2f - l\cdot\tan\phi}{2f + l\cdot\tan\phi} \tag{24}$$

At the same time, based on the cosine law, we have:

$$EE'^2 = ES^2 + E'S^2 - 2\cdot ES\cdot E'S\cdot\cos(\angle ESE') \tag{C9}$$

$$FF'^2 = FS^2 + F'S^2 - 2\cdot FS\cdot F'S\cdot\cos(\angle FSF') \tag{C10}$$

Where:

$$\angle ESE' = \angle FSF' = \angle GSG' = 2\beta \tag{C11}$$

$$\tan\beta = \frac{GO}{SO} = \frac{L/2}{d} \tag{C12}$$

Combining (C9) and (C10) we can get the relationship between EE' and FF' as follow:

$$\frac{EE'}{FF'} = \frac{\sqrt{L^2+4d^2} - L\cdot\tan\Gamma}{\sqrt{L^2+4d^2} + L\cdot\tan\Gamma} = \frac{\sqrt{l^2+4f^2} - l\cdot\tan\Gamma}{\sqrt{l^2+4f^2} + l\cdot\tan\Gamma} \tag{25}$$

In Fig.16, if we define (x_2, y_2), (x_o, y_o), (x_i, y_i) as the coordinates of point *E*, *O* and *I* on plane P_2 respectively, then we will get:

$$OE = \sqrt{(x_2 - x_o)^2 + (y_2 - y_o)^2} \tag{C13}$$

$$EI = \sqrt{(x_2 - x_i)^2 + (y_2 - y_i)^2} \tag{C14}$$

$$x_o = y_o = y_i \tag{C15}$$

$$x_i = -OI \tag{C16}$$

So we have:

$$x_2 = -OI/2 + (EI^2 - OE^2)/(2 \cdot OI) \tag{36}$$

$$y_2 = \sqrt{EI^2 - (OI + x_2)^2} \tag{37}$$

or

$$y_2 = -\sqrt{EI^2 - (OI + x_2)^2} \tag{38}$$

REFERENCES

[1] A. C. Kak and M. Slaney, "Principles of computerized tomographic imaging", *IEEE Press*, 1988.

[2] G. T. Gullberg, B. M. W. Tsui, C. R. Crawford, J. G. Ballard, and J. T. Hagius, "Estimation of geometrical parameters and collimator evaluation for cone beam tomography," *Med. Phys.*, vol. 17, no. 2, pp. 264–272,1990.

[3] J. Li, R. J. Jaszczak, H. Wang, K. L. Greer, and R. E. Coleman, "Determination of both mechanical and electronic shifts in cone beam SPECT," *Phys. Med. Biol.*, vol. 39, pp. 743–754, 1993.

[4] Ph. Rizo, P. Grangeat, and R. Guillemaud, "Geometric calibration method for multiple-head cone-beam SPECT system," *IEEE Trans. Nucl. Sci.*, vol. 41, pp. 2748–2757, July 1994.

[5] A.V. Bronnikov, "Virtual alignment of x-ray cone-beam tomography system using two calibration aperture measurements", *Opt. Eng*., vol.38, no.2, pp.381–386, 1999.

[6] D.Beque, J. Nuyts, G. Bormans, P. Suetens, and P. Dupont, "Characterization of pinhole SPECT acquisition geometry", *IEEE Trans.Med. Ima.*, vol.22, no.5,pp.599–612, May, 2003.

[7] M. Karolczak, S. Schaller, K. Engelke, A. Lutz, U. Taybenreuther, K. Wiesent, and W. Kalender, "Implementation of a cone-beam reconstruction algorithm for the single-circle source orbit with embedded misalignment correction using homogeneous coordinates", *Med. Phys.* 28 (10), pp. 2050–2069, October 2001.

[8] F. Noo, R. Clackdoyle, C. Mennessier, Timothy A White, and Timothy J Roney, "Analytic method based on identification of ellipse parameters for scanner calibration in cone-beam tomography", *Phys. Med. Biol.* 45 pp. 3489–3508, 2000.

[9] L. A. Feldkamp, L. C. Davis, and J. W. Kress, "Practical cone-beam algorithm", *J. Opt. Soc. Am. A*, Vol. 1, No. 6, pp 612-619, Jun. 1984.